Check for updates

Room-temperature yellow-orange (In,Ga,Al)P–GaP laser diodes grown on (n11) GaAs substrates

N. N. Ledentsov,[1,*] V. A. Shchukin,[1] Yu. M. Shernyakov,[2] M. M. Kulagina,[3] A. S. Payusov,[2] N. Yu. Gordeev,[2] M. V. Maximov,[2] A. E. Zhukov,[2] T. Denneulin,[4,5] and N. Cherkashin[5]

[1]*VI Systems GmbH, Hardenbergstr. 7, 10623 Berlin, Germany*
[2]*St. Petersburg Academic University, Khlopin St. 8/3, St. Petersburg 195220, Russia*
[3]*Ioffe Institute, Politekhnicheskaya 26, St. Petersburg 194021, Russia*
[4]*Peter Grünberg Institut (PGI–5), Wilhelm–Johnen–Straße, 52425 Jülich, Germany*
[5]*CEMES–CNRS, 29, rue Jeanne Marvig, BP 94347, 31055 Toulouse Cedex 4, France*
nikolay.ledentsov@v-i-systems.com

Abstract: Abstract: We report room temperature injection lasing in the yellow–orange spectral range (599–605 nm) in $(Al_xGa_{1-x})_{0.5}In_{0.5}P$–GaAs diodes with 4 layers of tensile-strained $In_yGa_{1-y}P$ quantum dot-like insertions. The wafers were grown by metal–organic vapor phase epitaxy side-by-side on (811), (211) and (322) GaAs substrates tilted towards the <111> direction with respect to the (100) surface. Four sheets of GaP-rich quantum barrier insertions were applied to suppress leakage of non-equilibrium electrons from the gain medium. Laser diodes having a threshold current densities of $\sim$7–10 kA/cm^2 at room temperature were realized for both (211) and (322) surface orientations at cavity lengths of $\sim$1mm. Emission wavelength at room temperature $\sim$600 nm is shorter by $\sim$8 nm than previously reported. As an opposite example, the devices grown on (811) GaAs substrates did not show lasing at room temperature.

References and links

1. H. Jorke and M. Fritz, "Stereo Projection Using Interference Filters," Proceedings of SPIE–IS&T Electronic Imaging, SPIE Vol. **6055**, 60550G (2006).
2. D. Bohn, "Intel made smart glasses that look normal," The Verge **2**, Feb. 5 (2018), *https://www.theverge.com/2018/2/5/16966530/intel-vaunt-smart-glasses-announced-ar-video*
3. N. Ledentsov and V. Shchukin, "Laser system for generation of colored three–dimensional images," US Patent Application Publication US20170332071A1 (2017).
4. P. Avci, A. Gupta, M. Sadasivam, D. Vecchio, Z. Pam, N. Pam, and M. R. Hamblin, "Low-level laser (light) therapy (LLLT) in skin: stimulating, healing, restoring," Semin. Cutan. Med. Surg. **32**(1), 41–52 (2013).
5. W. G. Telford, "Lasers in flow cytometry," Methods Cell Biol. **102**, 375–409 (2011).
6. S. Choudhary, K. Nouri, and M. L. Elsaie, "Photodynamic therapy in dermatology: a review," Lasers Med. Sci. **24**(6), 971–980 (2009).
7. M. Mueller, "Introduction to Confocal Fluorescence Microscopy, Tutorial Texts in Optical Engineering," SPIE Proceedings, Vol. **TT69** (2006).
8. K. A. Fedorova, M. A. Cataluna, P. R. Battle, C. M. Kaleva, I. L. Krestnikov, D. A. Livshits, and E. U. Rafailov, "Orange light generation from a PPKTP waveguide end pumped by a cw quantum–dot tunable laser diode," Appl. Phys. B **103**(1), 41–43 (2011).
9. K. A. Fedorova, G. S. Sokolovskii, D. I. Nikitichev, P. R. Battle, I. L. Krestnikov, D. A. Livshits, and E. U. Rafailov, "Orange-to-red tunable picosecond pulses by frequency doubling in a diode-pumped PPKTP waveguide," Opt. Lett. **38**(15), 2835–2837 (2013).
10. M. Dallesasse, D. W. Nam, D. G. Deppe, N. Holonyak, Jr., R. M. Fletcher, C. P. Kuo, T. D. Osentowski, and M. G. Craford, "Short–wavelength ($\leq$ 6400 Å) room□temperature continuous operation of *p–n* $In_{0.5}(Al_xGa_{1-x})_{0.5}P$ quantum well lasers," Appl. Phys. Lett. **53**(19), 1826–1828 (1988).

11. R. V. Chelakara, M. R. Islam, J. G. Neff, K. G. Fertitta, A. L. Holmes, F. J. Ciuba, and R. D. Dupuis, "Growth of high–quality InAlP/InGaP quantum wells and InAlP/InGaP superlattice barrier cladding layers by metalorganic chemical vapor deposition," J. Cryst. Growth **145**(1–4), 179–186 (1994).

12. R. V. Chelakara, M. R. Islam, J. G. Neff, K. G. Fertitta, A. L. Holmes, F. J. Ciuba, R. D. Dupuis, T. A. Richard, N. Holonyak, Jr., and K. C. Hsieh, "Short–wavelength room–temperature continuous–wave laser operation of InAlP–InGaP superlattices grown by metalorganic chemical vapor deposition," Appl. Phys. Lett. **65**(7), 854–856 (1994).

13. W. J. Choi and P. D. Dapkus, "Low threshold 630 nm band AlGaInP diode laser with AlAs native oxide current aperture," IEEE LEOS Annual Meeting Conference Proceedings **2**, 533–534 (1999).

14. W. R. Hitchens, N. Holonyak, Jr., P. D. Wright, and J. J. Coleman, "Low–threshold LPE $In_{1-x}Ga_xP_{1-z}As_z/In_{1-x}Ga_xP_{1-z}As_z/In_{1-x}Ga_xP_{1-z}As_z$ yellow double–heterojunction laser diodes ($J < 10^4$ A/cm^2, $\lambda \sim 5850$ Å, 77°K)," Appl. Phys. Lett. **27**(4), 245–247 (1975).

15. M. Ikeda, M. Honda, Y. Mori, K. Kaneko, and N. Watanabe, "Yellow–emitting AlGaInP double heterostructure laser diode at 77 K grown by atmospheric metalorganic chemical vapor deposition," Appl. Phys. Lett. **45**(9), 964–965 (1984).

16. X. A. Valster, M. N. Finke, M. J. B. Boermans, J. M. M. V. D. Heijden, C. J. G. R. Spreuwenberg, and C. T. H. F. Liedenbaum, "Green (555 nm) Continuous Wave Lasing Emission (77 K) of GaInP/AlGaInP Multiple Quantum Well Laser Diodes," 12th Int. Semiconductor Laser Conf. (Davos, Switzerland), Post–deadline paper vol. PD–12, p. 25 (1990).

17. N. N. Ledentsov, V. A. Shchukin, J. Lyytikäinen, O. Okhotnikov, Yu. M. Shernyakov, A. S. Payusov, N. Yu. Gordeev, M. V. Maximov, S. Schlichting, F. Nippert, and A. Hoffmann, "Green (In,Ga,Al)P–GaP light–emitting diodes grown on high–index GaAs surfaces," Appl. Phys. Lett. **105**(18), 181902 (2014).

18. N. N. Ledentsov, V. A. Shchukin, J. Lyytikäinen, O. Okhotnikov, N. A. Cherkashin, Yu. M. Shernyakov, A. S. Payusov, N. Yu. Gordeev, M. V. Maximov, S. Schlichting, F. Nippert, and A. Hoffmann, "Green (In,Ga,Al)P–GaP Light–Emitting Diodes grown in high–index GaAs surfaces," Proc. SPIE **9383**, 93830E (2015).

19. N. N. Ledentsov, V. A. Shchukin, Yu. M. Shernyakov, M. M. Kulagina, A. S. Payusov, N. Yu. Gordeev, M. V. Maximov, and N. A. Cherkashin, "(In,Ga,Al)P–GaP laser diodes grown on high–index GaAs surfaces emitting in the green, yellow and bright red spectral range," Semicond. Sci. Technol. **32**(2), 025016 (2017).

20. H. Hamada, K. Tominaga, M. Shono, S. Honda, K. Yodoshi, and T. Yamaguchi, "Room temperature CW operation of 610 nm band AlGaInP strained multiquantum well laser diodes with multiquantum barrier," Electron. Lett. **28**, 1834–1836 (1992).

21. T. Tanaka, H. Yanagisawa, M. Takimoto, and S. Minagawa, "Tensile–strained AlGaInP single quantum well LDs emitting at 615 nm," Electron. Lett. **29**(21), 1864–1866 (1993).

22. P. D. Bour, D. W. Treat, K. J. Beernink, B. S. Krusor, R. S. Geels, and D. F. Welch, "610–nm band AlGaInP single quantum well laser diode," IEEE Photonics Technol. Lett. **6**(2), 128–131 (1994).

23. H. Hamada, "Characterization of gallium indium phosphide and progress of aluminum gallium indium phosphide system quantum–well laser diode," Materials (Basel) **10**(8), 875 (2017).

24. J. A. Lott and K. J. Malloy, "Orange vertical cavity surface emitting lasers," in CLEO/Pacific Rim '95, Pacific Rim Conference on Lasers and Electro–Optics (OSA, 1995), pp. 258–259.

25. M. A. Majid, A. A. Al-Jabr, R. T. Elafandy, H. M. Oubei, M. S. Alias, B. A. Alnahhas, D. H. Anjum, T. Kh. Ng, M. Shehata, and B. S. Ooi, "First demonstration of orange–yellow light emitter devices in InGaP/InAlGaP laser structure using strain–induced quantum well intermixing technique," Proc. SPIE **9767**, 97670A (2016).

26. N. Cherkashin, S. Reboh, M. J. Hÿtch, A. Claverie, V. V. Preobrazhenskii, M. A. Putyato, B. R. Semyagin, and V. V. Chaldyshev, "Determination of stress, strain, and elemental distribution within In(Ga)As quantum dots embedded in GaAs using advanced transmission electron microscopy," Appl. Phys. Lett. **102**(17), 173115 (2013).

27. R. Nötzel, N. N. Ledentsov, L. Däweritz, M. Hohenstein, and K. Ploog, "Direct synthesis of corrugated superlattices on non-(100)-oriented surfaces," Phys. Rev. Lett. **67**(27), 3812–3815 (1991).

28. I. L. Krestnikov, M. Strassburg, M. Caesar, A. Hoffmann, U. W. Pohl, D. Bimberg, N. N. Ledentsov, P. S. Kop'ev, Zh. I. Alferov, D. Litvinov, A. Rosenauer, and D. Gerthsen, "Control of the electronic properties of CdSe submonolayer superlattices via vertical correlation of quantum dots," Phys. Rev. B **60**(12), 8695–8703 (1999).

29. N. Cherkashin, T. Denneulin, and M. J. Hÿtch, "Electron microscopy by specimen design: application to strain measurements," Sci. Rep. **7**(1), 12394 (2017).

30. S. Tiwari and D. J. Frank, "Empirical fit to band discontinuities and barrier heights in III–V alloy systems," Appl. Phys. Lett. **60**(5), 630–632 (1992).

31. Ch. G. Van de Walle, "Band lineups and deformation potentials in the model-solid theory," Phys. Rev. B Condens. Matter **39**(3), 1871–1883 (1989).

32. N. N. Ledentsov and V. A. Shchukin, "Novel concepts for injection lasers," SPIE Opt. Eng. **41**(12), 3193–3203 (2002).

33. N. N. Ledentsov, V. A. Shchukin, M. V. Maximov, N. Yu. Gordeev, N. A. Kaluzhniy, S. A. Mintairov, A. S. Payusov, and Yu. M. Shernyakov, "Optical Mode Engineering and High Power Density per Facet Length (>8.4 kW/cm^2) in Tilted Wave Laser Diodes," Proc. SPIE **9733**, 97330P (2016).

34. H. Tanaka, Yu. Kawamura, and H. Asahi, "Refractive indices of $In_{0.49}Ga_{0.51-x}Al_xP$ lattice matched to GaAs," J. Appl. Phys. **59**(3), 985–986 (1986).

35. M. V. Maximov, Yu. M. Shernyakov, I. I. Novikov, S. M. Kuznetsov, L. Ya. Karachinsky, N. Yu. Gordeev, V. P. Kalosha, V. A. Shchukin, and N. N. Ledentsov, "High–Performance 640–nm–Range GaInP–AlGaInP Lasers Based on the Longitudinal Photonic Bandgap Crystal with Narrow Vertical Beam Divergence," IEEE J. Quantum Electron. **41**(11), 1341–1348 (2005).
36. Zh. Deng, J. Ning, R. Wang, Zh. Su, Sh. Xu, Zh. Xing, Sh. Lu, J. Dong, and H. Yang, "Influence of temperature and reverse bias on photocurrent spectrum and supra–bandgap spectral response of monolithic GaInP/GaAs double–junction solar cell," Front. Optoelectron. **9**(2), 306–311 (2016).

1. Introduction

A variety of modern applications requires compact low–cost wavelength–adjustable or wavelength–tunable coherent light sources emitting in the deep green, yellow and bright red spectral ranges. One class of applications is related to three–dimensional (3D) laser displays, for example, based on Wavelength Multiplex Technology [1], laser–illuminated glasses for augmented or virtual reality [2] and laser–based systems with wavelength–sensitive focal lengths for generating glass–free 3D images [3]. In particular, bright red and yellow–orange (< 620 nm) multi–wavelength lasers are needed. Yellow–orange light sources are needed in dermatology [3], biophotonics [4], photomedicine [5], confocal fluorescence microscopy [6] and other bio–medical applications. Commercially available lasers of this spectral range are mostly based on frequency doubling of the laser light from an infrared laser diode by means of a nonlinear crystal [7]. The devices are complex and bulky and the wavelength adjustment is limited to only a few selected wavelengths [8, 9].

InGaAlP–based laser diodes were considered as promising candidates [10–13] for providing emission in bright–red to yellow–orange spectral range. Indeed, lasing emission in the yellow spectral range was demonstrated at 77 K [14, 15]. However, the threshold current density was too high (~6 kA/cm^2) even at low temperature making such devices not suitable for practical applications. More recently injection lasing at 555 nm at 77 K [16] was reported applying 16–fold stacked ultrathin (1.4 nm) $In_{0.5}Ga_{0.5}P$ insertions separated by $(Al_{0.5}Ga_{0.5})_{0.5}In_{0.5}P$ 4 nm–thick barrier layers. The lasing was observed in narrow stripe (7 μm) devices and the highest operation temperature was 150 K in the pulsed mode. However, no information was provided on the substrate orientation, the compositions and thicknesses of the cladding layers used for the optical and electron confinement, the cavity length and facet coating. Recently, it was reported that (In,Ga,Al)P light–emitting diodes grown on high–index GaAs substrates inclined from (100) towards <111>–crystallographic direction and containing tensile strained ultrathin GaP insertions showed an improved intensity of the electroluminescence at room temperature in the green spectral range of ~568 nm [19] as compared to (100)–grown devices [17, 18]. The effect was attributed to the enhanced barrier heights in the conduction band for ultrathin tensile strained GaP barriers formed on surfaces close to the (111) GaAs orientation. To reach room–temperature lasing in (In,Ga,Al)P system, different variations of the structures and of the active medium were applied. Multiple compressively strained AlGaInP quantum well (QW) structure [20] and single tensile strained AlGaInP QW [21] allowed reaching continuous wave (CW) lasing at 615 nm. Using a single compressively strained GaInP QW [22] resulted in lasing in the pulsed mode at 614 nm in broad area devices. In the recent review [23] it was emphasized that 615 nm is in the shortest wavelength–range at which room–temperature lasing was reported for (In,Ga,Al)P–GaAs edge–emitting lasers. Same wavelength limitation was reported for vertical–cavity surface–emitting lasers [24]. Very recently injection lasing at 608 nm was achieved at room temperature in laser structures subjected to high–temperature strain–induced intermixing [25]. We note that the possibility to realize room temperature lasing in the yellow spectral range (586 nm) by optical pumping was demonstrated already in 1994 [12], once efficient heat dissipation could be provided. In the present paper we demonstrate a further significant advance towards yellow and green spectral range allowing 600 nm lasing wavelength in broad area devices.

2. Growth and structural characterization

The structures studied in the present work were grown using metal–organic vapor phase epitaxy (MOVPE) on (811)A, (211)A and (322)A GaAs Si–doped substrates (n~2 × 10^{18} cm^{-3}). First, a 0.3 µm–thick Si–doped (10^{18} cm^{-3}) GaAs buffer layer was epitaxially grown to achieve reproducible surface morphology. Following the formation of the buffer layer, a Si–doped (n~1x10^{18} cm^{-3}) 1 µm–thick indirect gap $(Al_{0.8}Ga_{0.2})_{0.5}In_{0.5}P$ cladding layer was deposited. Afterwards, a coupled waveguide containing a passive part, an intermediate thin cladding layer and an active waveguide containing multiple QW structure was grown. The gain medium consists of four tensile–strained $In_xGa_{1-x}P$ (x~38–40%) insertions separated by lattice matched $(Al_{0.5}Ga_{0.5})_{0.5}In_{0.5}P$ layers. Multiple GaP–rich insertions were introduced into the p–cladding layer as blocking barriers for electrons just after the initial 2 nm–thick $(Al_{0.8}Ga_{0.2})_{0.5}In_{0.5}P$ cap formed on top of the active layer. Four GaP–rich insertions, each 2 nm–thick, were separated by $(Al_{0.8}Ga_{0.2})_{0.5}In_{0.5}P$ layers having thicknesses of 10 nm, 7 nm, and 5 nm. Different thicknesses of the layers between barriers were applied specifically to avoid possible tunneling effects through resonant QW energy levels. Thus, the entire structure with multiple GaP–rich insertions acts as a single 30 nm–thick barrier. The barrier structure was followed by a p–doped $(Al_{0.8}Ga_{0.2})_{0.5}In_{0.5}P$ cladding layer (5x10^{17} cm^{-3}). Finally, a 0.2 µm–thick Be–doped (10^{18} cm^{-3}) GaAs contact layer was deposited on top. InGaAlP regions were grown at ~750°C, and GaAs regions at ~700°C.

Figure 1 shows out–of–plane ε_{zz} in Fig. 1(a) and 1(b) and in–plane ε_{xx} in Fig. 1(c) and 1(d) strain maps which were obtained in two orthogonal cross–sections (1–10) (Fig. 1(a) and 1(c)) and (11–1) (Fig. 1(b) and 1(d)) over the four nominally 2 nm–thick $Ga_{0.6}Al_{0.15}In_{0.25}P$ barrier insertions in the structure grown on (112) GaAs substrate. The strain maps were extracted with respect to the $Ga_{0.21}Al_{0.30}In_{0.49}P$ lattice with a spatial resolution of 1 nm for ε_{zz} and of 2 nm for ε_{xx} by applying dark–field electron holography (DFEH) in high–resolution (HR) mode [19, 26] at I2TEM–Toulouse, a HF3300 (Hitachi) TEM operating at 300 kV. The ε_{zz} maps of the barriers indicate that the 4 nm–thick in–plane tensile strained layers contain about 40% of indium that was deduced by using elasticity theory and Vegard's law. We note that some broadening of the interfaces and Indium intermixing with the surrounding matrix can be attributed (at least partially) to the periodic interface corrugation of the (112) surface [27], as even submonolyaer GaP insertions could be resolved in similar structures grown on the (118) surface [17, 18]. The ε_{xx} maps in the barriers demonstrate the presence of vertical column–like in–plane strain variation with amplitude of ~ ± 0.2% and a period of ~30 nm. Such in–plane strain variation again can be provoked by the (112) surface corrugation and results in vertically–correlated arrangements similar to those observed in [28].
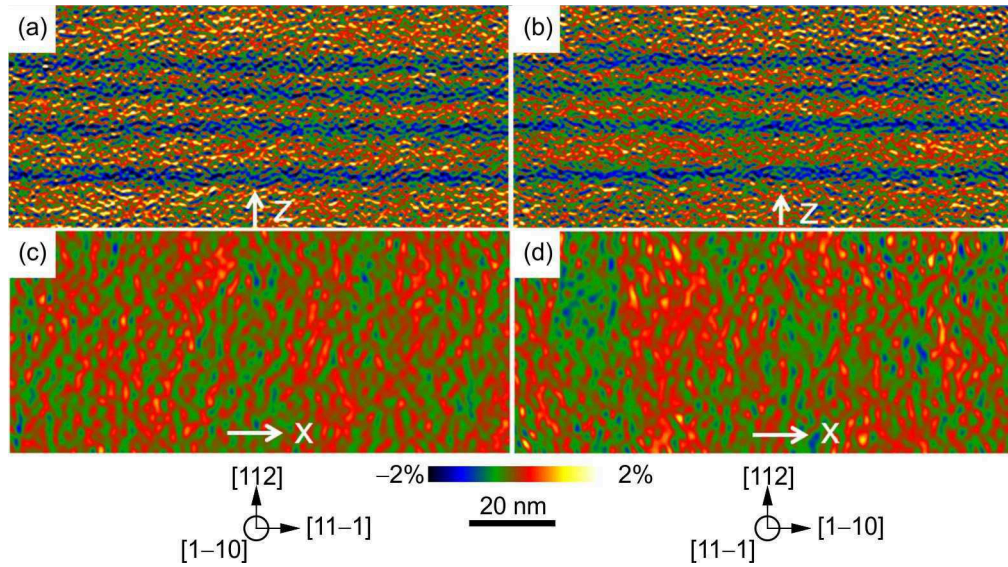
Fig. 1. (a), (b) Out–of–plane ε_{zz} and (c), (d) in–plane ε_{xx} strain distributions in four nominally 2 nm–thick $Ga_{0.6}Al_{0.15}In_{0.25}P$ barrier insertions in the structure grown on (112) GaAs substrate. Strain was extracted by dark–field electron holography in high–resolution mode with respect to $Ga_{0.21}Al_{0.30}In_{0.49}P$ lattice with a 1 nm (a), (b) and 2 nm (c), (d) spatial resolution in two orthogonal cross–sections: (a), (c) (1–10); (b), (d) (11–1). Note column–like ε_{xx} strain variation in both cross–sections.

Strain distribution in the gain medium of the (112) structure which contains four tensile strained nominally 4–nm thick $In_{0.4}Ga_{0.6}P$ layers was extracted by applying Moiré by Specimen Design (MoSD) technique [29]. The experiment involving double lamella specimen was realized at an old generation Jeol 2010 TEM operating at 200 kV equipped with 1.3K x 1K CCD camera. Figures 2(a) and 2(c) show ε_{zz} and ε_{xx} maps extracted from moiré images with respect to the $Ga_{0.21}Al_{0.30}In_{0.49}P$ lattice with a 4 nm spatial resolution. The analysis of Fig. 2(a) indicates that the tensile strained QWs have a wavy morphology, repeating from the bottom to the upmost layers, with a lateral period of 50 nm and a thickness varying from 4 nm to 8 nm. We detect in–plane column–like strain variation with an amplitude of ~–0.6% and + 0.6% at the thickest and the thinnest parts of the QWs, respectively (Fig. 2(c)) which is accompanied with the ε_{zz} strain variation from –1.2% to – 0.4%. We have applied 2D finite element method (FEM) modelling (Fig. 2(b) and 2(d)) with the aim to deduce In composition within such complex structures. The QWs were approximated by laterally connected triangular shape wires with a constant In composition. A good quantitative agreement between the experimental and simulated ε_{zz} maps has been obtained for wires containing 40% of Indium. While principally good qualitative agreement has been obtained also between ε_{xx} maps, the amplitude of the simulated in–plane strain variation of ~ ± 0.2% (Fig. 2(d)) is lower than that found in the experiment (Fig. 2(c)). We believe that such discrepancy is related to the limits of the QWs morphology applied in the simplified 2D model: one would expect a much stronger in–plane strain relaxation at the apexes of the 3D islands if they would have been introduced into the 3D model. In conclusion, we evidenced that the tensile strained layers contain laterally connected 50 nm– large 8 nm–high islands containing 40% of indium which are vertically correlated.
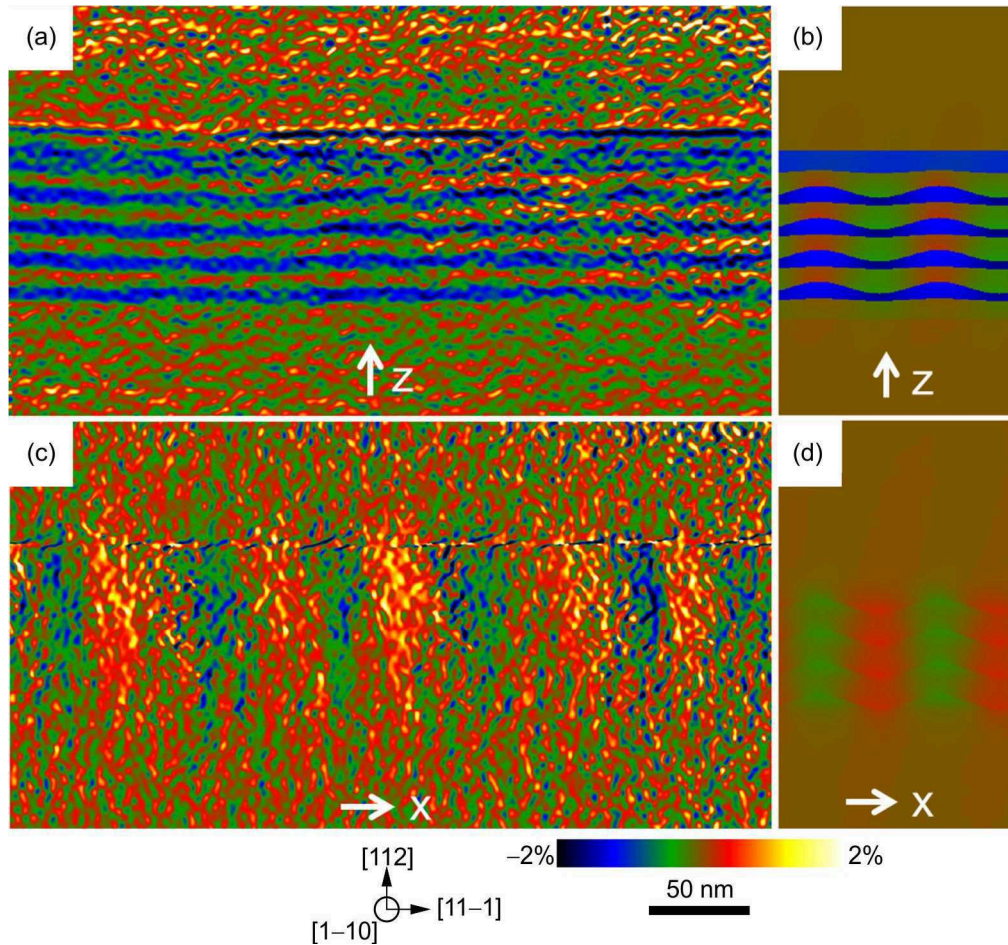
Fig. 2. (a) Out–of–plane ε_{zz} and (c) in–plane ε_{xx} strain distributions in the gain medium of the (112) structure which contains four tensile strained nominally 4–nm thick $In_{0.4}Ga_{0.6}P$ layers. Strain was extracted with respect to $Ga_{0.21}Al_{0.30}In_{0.49}P$ lattice with a 4–nm spatial resolution by applying moiré by specimen design technique in cross–section (1–10). (b) Out–of–plane ε_{zz} and (d) in–plane ε_{xx} strain distributions obtained by finite element method modelling. Note column–like ε_{xx} strain variation both in (c) and (d).

Finally, the structures grown on the (112) and (223) GaAs substrates both contain vertically–coupled arrays of islands (QDs) that was identified in two orthogonal in–plane directions. It should be emphasized that no evidence of atomic–scale ordering was found. As opposite, (811)A–grown structure demonstrated spontaneous formation of natural tilted superlattices in the alloy as was already previously observed and discussed [15]. The QWs were revealed in form of corrugated quantum wire–like structures with a lateral periodicity of ~35 nm.

To address the effect of the island–like nature of the active medium on carriers, it is worth estimating the modulation amplitude of the potential for electrons and holes. Spatial quantization of electrons in the vertical direction yields the energy in the thick parts of the GaInP layers, (thickness ~8 nm) ~250 meV lower than in the thin parts (between islands) where the thickness is ~4 nm. An increase in Indium composition and tensile strain between the islands contribute in the opposite direction. The estimation of the effect using materials parameters from [30, 31] yields ~190 meV. The overall effect shows the localization potential for electrons ~60 meV deeper in the islands than in the domains of the GaInP layers between the islands. Thus the islands in the active medium should act as quantum dots also at room

temperature. We can mention that the QD potential suppresses diffusion of nonequilibrum carriers towards point defects and surface defects and thus can improve the reliability of the device. We also note that the spectral width of the electroluminescence spectra (16–19 nm full width at half maximum) indicated a good average uniformity of the QD array and the impact of inhomogeneous broadening should not be dominant.

As noted for the structure grown side by side on (811)A substrate self–organized corrugated quantum wire arrays were observed in the gain region, as it was already discussed previously [15, 18]. The (811)A–grown structure emitted however at ~15 nm longer wavelengths than those grown on (211) and (322) and demonstrated no lasing at room temperature. This observation is in general agreement with lower efficiency of GaP–rich barriers for substrate orientations relatively weakly inclined from the (100) plane. Thus this structure will not be discussed further in the present paper. We also note that, as the formation of nanostructures proceeded in entirely self–organized mode, there was no option of direct comparison of the structures studied in the present paper to QW structures of the same design grown on similarly–oriented substrates.

3. Electroluminescence and lasing

As explained in Refs [18]. and [19], the vertical epitaxial design was aimed at achieving a reduced vertical beam divergence [32]. We apply tilted wave laser (TWL) concept [33] which is basically similar to the couple cavity design with a passive waveguide section matching the $\lambda/2$ condition. A full width at half maximum of 25° was targeted; the refractive indices were taken from Ref [34]. Thick waveguide concept is chosen for short wavelength (In,Ga,Al)P laser diodes because catastrophic optical mirror damage plays a key role in degradation of such devices. We note that the effective refractive indices of the strained quantum wells (QWs) used in the modelling were well studied for (811)–oriented structures [35].

The devices for the electroluminescence (EL) studies were processed in ridge–stripe geometry with 50 μm stripes. The stripes were oriented in the surface plane in such direction that the laser facets perpendicular to the stripes matched to the cleavage planes (01–1). Cavity length of 1 mm and uncoated facets were used. The contact resistance was ~$5 \times 10^{-4} \ \Omega \ cm^2$. The devices were mounted p–side down onto a copper heat sink with indium solder and tested in the pulsed mode at 300 ns pulse duration and 1 kHz repetition rate. The EL spectra and intensity were recorded. For temperature studies the devices on copper submounts were introduced into a transparent glass Dewar in between of the resistive coil furnace and liquid nitrogen partially filling the bottom part of the Dewar. The temperature of the laser heat sink was controlled by a thermocouple.

Figure 3 demonstrates room–temperature EL spectra at different drive currents for laser diodes on (a) (211) substrate and (b) (322) substrate. Threshold current densities for 1 mm cavity length were at ~7–12 kA/cm^2 at room temperature and were controlled by external losses. As it will be illustrated below, a strong superliner growth of the EL intensity was recorded at current densities exceeding 400 A/cm^2. This observation indicates that, with proper processing and optimization of external losses, the performance of the devices can be improved. The lasing wavelength varied across the wafer within 599–604 nm for both substrate orientations.
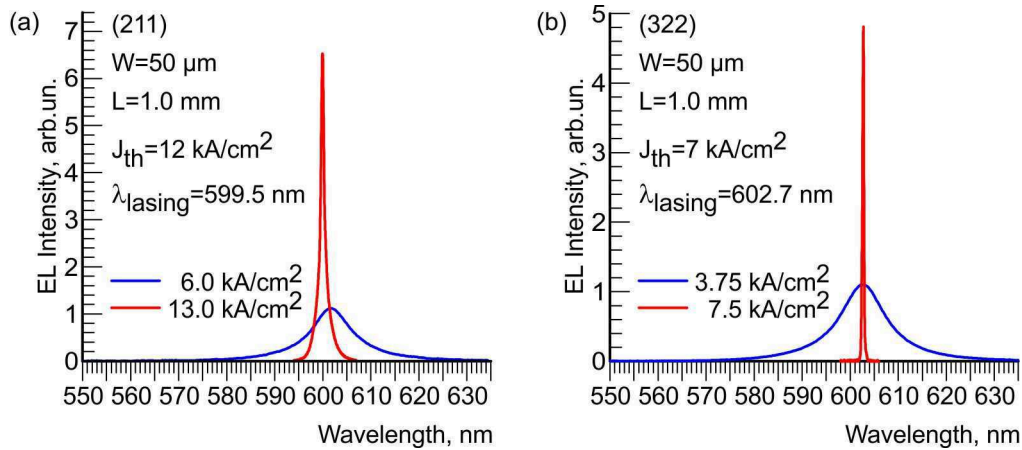
Fig. 3. Room temperature electroluminescence (EL) spectra at different drive currents for laser diodes grown on (a) (211) substrate and (b) (322) substrate.

Vertical and lateral far field patterns of the device grown on (211) GaAs substrate are shown in Fig. 4(a) and 4(b), respectively. The device is clearly single mode in the vertical direction (fast axis) and the full width at half maximum (FWHM) matches well the modeled value (FWHM~25°).
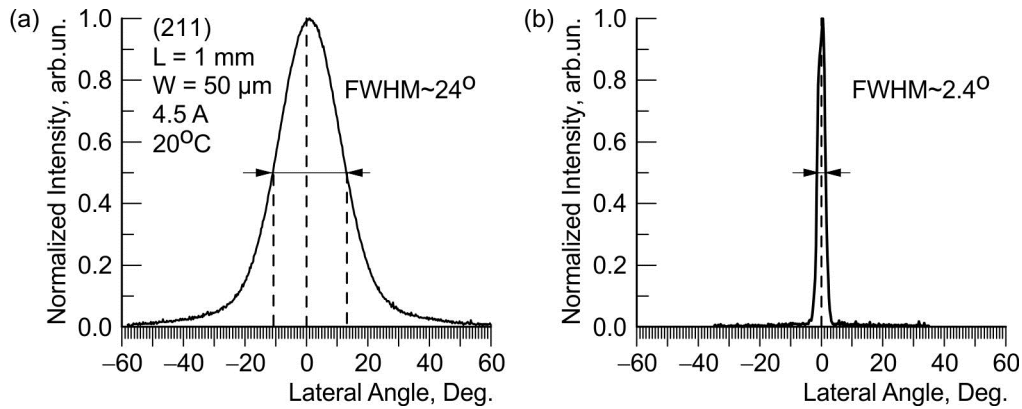

Fig. 4. Room–temperature vertical (a) and lateral (b) far field pattern of the (211)–grown laser.

Figure 5 displays light–current characteristics of the broad–stripe lasers at pulsed currents. A clear threshold current for the lasing process is revealed both for (211) and (322) substrates. As no facet passivation was applied, the maximum optical power reached was limited to ~800 mW. Upon further power increase a catastrophic degradation of the devices occurred due to the facet overheating and damage (catastrophic optical mirror damage, COMD). To prevent this effect one needs to passivate the facets and reduce external losses, and, thus, the nonequilibrium carrier density at threshold, by depositing high reflectivity coating at least on the rear facet of the device and preferably fabricate narrow stripes to improve heat dissipation. However already in the pulsed mode the average power reached in Fig. 5 constituted 0.32 mW. At higher duty cycles, by keeping the pulse duration and by increasing the repetition frequency from 4 kHz to 40 kHz it became possible to reach higher average power levels ~1 mW, already sufficient for important practical applications at 600 nm wavelength such as virtual/augmented reality glasses and helmets [2].
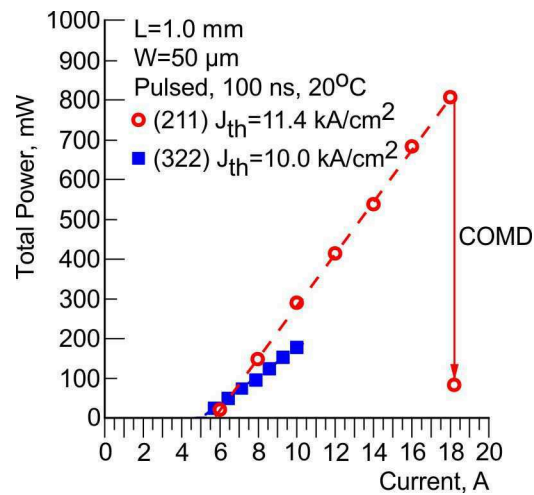
Fig. 5. Light–current characteristics of laser diodes grown on (322) and (211) substrates. (322) structure was not explored at power levels close to catastrophic optical mirror damage (COMD).

Figure 6 presents EL spectra of (211)–laser at different current densities. A strong superlinear increase of the maximum intensity is observed at higher current densities and is accompanied by the narrowing of the EL emission. The EL band of stimulated emission and lasing is Stokes–shifted from the bandgap feature resolved at low excitation densities.
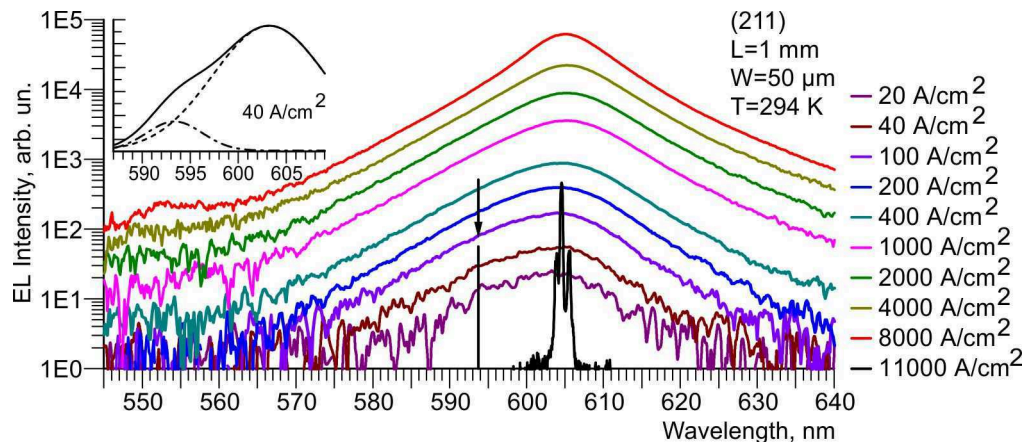

Fig. 6. EL spectrum of (211) laser at different current densities. A strong superlinear growth of the intensity is observed at current densities above 400 A/cm². The band of stimulated emission and lasing is Stokes–shifted from the bandgap feature resolved at low excitation densities. The insert shows the deconvoluted EL spectrum at 40 A/cm² in linear scale revealing a bandedge emission with the maximum at 603.5 nm (dashed line) and emission at a shorter wavelength with the maximum at 594 nm (dash–dotted line). Lasing spectrum is not to scale.

Figure 7 shows the temperature dependence (a) of the emission wavelength of the lasing emission and of the bandgap EL feature and (b) of the threshold current density obtained for the laser structure grown on (211)A GaAs substrate. We note that while the bandgap feature shifts in the range 100–295 K by ~70 meV (Fig. 7(b)) in agreement with the trend for the bandgap photoluminescence of (In,Ga)P layers on GaAs [23, 36], the spectral shift of the stimulated emission and lasing is much stronger and the Stokes shift becomes more pronounced upon temperature increase. We tentatively attribute the effect to the multi–particle effects and contribution of phonons, which becomes stronger once the temperature

increases and the exciton transport between QDs becomes significant. More detailed studies will be published elsewhere. The dependence of the threshold current density on the heat sink temperature is shown in Fig. 7(b). The device provides high temperature stability up to temperatures ~220 K (T_0~165 K) while at higher temperatures the temperature stability is reduced (T_0~31 K).
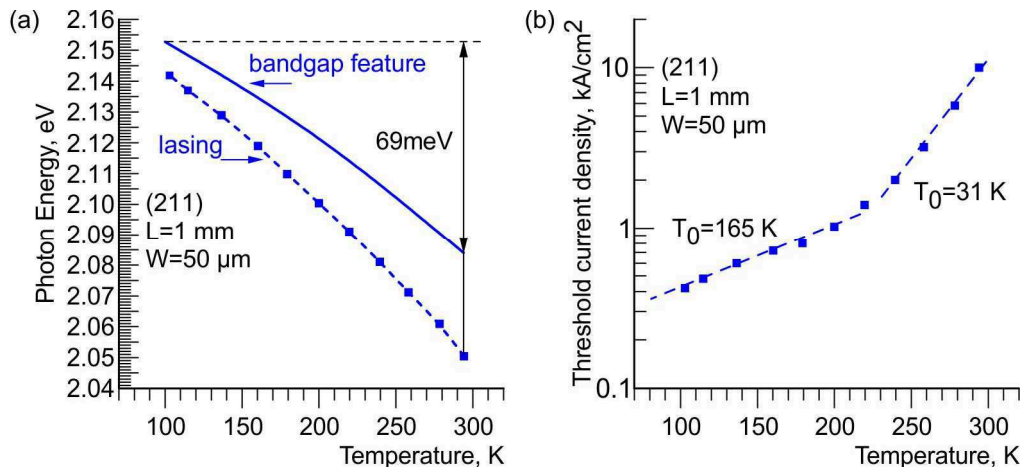

Fig. 7. Temperature dependence of (a) the photon energy of the emitted light for the bandedge EL and of the bandgap energy and (b) of the threshold current density for laser diode grown on (211) substrate.

We attempted to further shift lasing emission towards green–yellow spectral range by optimizing the wavelength of the gain medium. Lasing at 559 nm at 85 K was reached both for (211)– and (322)–oriented substrates. The bandedge EL was recorded for both structures at 570–575 nm. The threshold current density at this temperature was lower for (322)–oriented structure (700 A/cm^2 vs ~1500 A/cm^2). The lasing at 10 kA/cm^2 could be realized up to ~130 K for (211) substrate and up to 160 K for (322) substrate. Even no lasing at room temperature was observed in this case, one can expect that, with further optimization of the design using GaP–rich tensile–trained barrier insertions and applying bandgap engineering of the QDs, a further shift towards green–yellow lasing may become possible.

4. Conclusions

To conclude, we have proposed and developed advanced approach aimed to extend lasing wavelength of (In,Ga,Al)P–based laser diodes towards yellow–orange and, further, to green–yellow spectral range. A combination of the epitaxial growth on high–index GaAs substrates, strongly inclined from (100) surface towards <111> direction, namely, on (211) and (322) substrates, on the one hand, and employing tensile strained GaP–rich barriers, acting as current blocking layers for non–equilibrium electrons, the height of the barriers significantly increasing for these orientations, on the other hand, has allowed reaching lasing at ~599–605 nm at room temperature. Using a different active medium has allowed green–yellow lasing up to 160 K. Further optimization of the active medium and barriers may suggest both a further improvement of the characteristics of yellow–orange lasers and a possibility to reach green lasing at room temperature.